Volume 59(Suppl.2):303-321, 2015
Acta Biologica Szegediensis
http://www.sci.u-szeged.hu/ABS

REVIEW

Micro- and nanotechnology for cell biophysics

Péter Galajda, Lóránd Kelemen*, Gergely A. Végh

Institute of Biophysics, Biological Research Centre of the Hungarian Academy of Sciences, Szeged, Hungary

ABSTRACT Procedures and methodologies used in cell biophysics have been improved tremendously with the revolutionary advances witnessed in the micro- and nanotechnology in the last two decades. With the advent of microfluidics it became possible to reduce laboratory-sized equipment to the scale of a microscope slide allowing massive parallelization of measurements with extremely low sample volume at the cellular level. Optical micromanipulation has been used to measure forces or distances or to alter the behavior of biological systems from the level of DNA to organelles or entire organisms. Among the main advantages is its non-invasiveness, giving researchers an invisible micro-hand to "touch" or "feel" the system under study, its freely and very often quickly adjustable experimental parameters such as wavelength, optical power or intensity distribution. Atomic force microscopy (AFM) opened avenues for in vitro biological applications concerning with single molecule imaging, cellular mechanics or morphology. As it can operate in liquid environment and at human body temperature, it became the most reliable and accurate nanoforce-tool in the research of cell biophysics. In this paper we review how the above three techniques help increase our knowledge in biophysics at the cellular level.
Acta Biol Szeged 59(Suppl.2):303-321 (2015)

KEY WORDS

atomic force microscopy
low Reynolds number
microfluidics
optical micromanipulation
optical tweezers

Microfluidics

Introduction

Microfluidics is an emerging technology that deals with the manipulation of liquids on the microscale. Such techniques may contribute to the advance of various scientific fields, such as chemistry, materials science, physics and biology. From the vast spectrum of applications, in this review we focus on the use of fluid microtechnologies in the biological research. The last two decades saw an impressing development of microfluidics with more and more research labs embracing this technique. This is due to several key advantages that are associated with small size: low sample volume needed, possibility cellular scale measurements, possibility of massive parallelization and automation. Furthermore microscale fluidic phenomena are widespread in nature. Miniature capillaries play an important role in blood circulation of higher organisms or in the water transport in plants. Small cavities between soil particles are habitats for countless microbes. Biofilms formed by bacteria often constitute a complex fluidic network (Stoodley et al. 1994) which assures the proper nutrition supply over the whole structure. Microfluidics not only makes it possible to reproduce such natural structures in an engineered manner in a laboratory experiment, but also to use the special characteristics of microscale hydrodynamics (e.g., the lack of turbulence, and the significance of diffusion) for experiments that could not be done on macroscale.

Furthermore commercial equipment and methods appeared lately incorporating microfluidic elements (digital PCR, single cell analytic techniques, *etc*.).

Basics of microfluidics

Microfluidic structures consist of channels and chambers with some characteristic dimensions in the range of 500 μm-100 nm (Fig. 1). The basic equation describing the hydrodynamics of (incompressible) fluid flow is the Navier-Stokes equation (Acheson 1990) (Eq. 1).

$$\rho\left(\frac{\partial \boldsymbol{v}}{\partial t} + \boldsymbol{v}\cdot\boldsymbol{\nabla}\boldsymbol{v}\right) = -\boldsymbol{\nabla}p + \mu\boldsymbol{\nabla}^{2}\boldsymbol{v} + \boldsymbol{f} \quad \text{Eq. 1}$$

Here ρ is the mass density of the fluid, v is the velocity vector of a fluid element, p is the local pressure, μ is the fluid viscosity and f represents external forces. The left side of eq. 1 describes inertial forces (due to unsteady and convective acceleration represented by the two terms in the parenthe-

Submitted Jan 10, 2015; Accepted Aug 28, 2015
*Corresponding author. E-mail: kelemen.lorand@brc.mta.hu

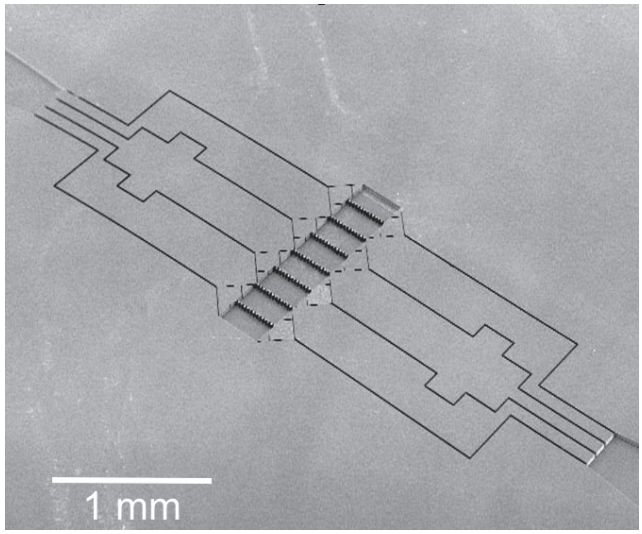

Figure 1. A microfluidic chip consisting of channels and chambers etched into a silicon substrate.

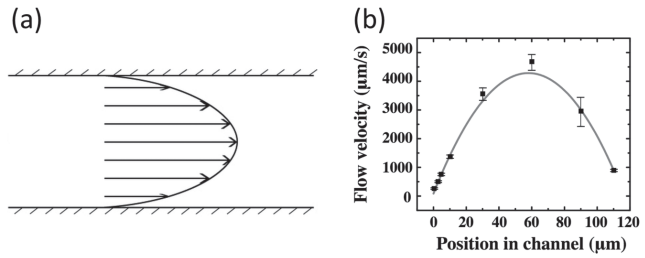

Figure 2. Flow in a channel. (a) The solution of the Navier-Stokes equation yields a parabolic velocity profile in a tubular channel. (b) The flow velocity profile measured in a 120 μm wide and 120 μm deep microchannel using particle imaging velocimetry. A parabolic fit is given to the measurement points.

sis). The right side includes the forces emerging from the divergence of stress (due to the pressure gradient and viscous effects) besides the external forces. By solving this equation one obtains the local velocity vector of the fluid by which the flow can be fully described. For example, solving the Navier-Stokes equation for a flow in a pipe, with non-stick boundary condition (the fluid is stationary at the wall) results a parabolic flow profile across the width of the pipe (Fig. 2). The flow profile must be taken into account in some biological experiments. For example some cells are very sensitive to shear stress. Exposed to large flow velocity gradients such cells may be greatly affected by the mechanical stress arising due to the flow.

The Hagen-Poiseuille equation (Kirby 2010) expresses the relation between the pressure drop and the pipe diameter (among some other parameters) for a tubular flow (Eq. 2).

$$\Delta p = \frac{8\mu L Q}{\pi r^4} \qquad \text{Eq. 2}$$

Here L is the length of the pipe, Q is the volumetric flow rate and r is the pipe radius. There is a very strong, quadratic dependence of the pressure drop (necessary to drive the flow) and the pipe radius. Therefore, significantly higher pressure is needed to push the liquid through small holes than larger openings, even if the total cross section areas are the same. One can experience this when pressing liquid through a syringe filter, for example. Furthermore, the Hagen-Poiseuille equation suggest that extremely large pressures may be needed to drive liquid through tiny microchannels, which in some cases may be inadequate in biological experiments.

Some degree of characterization of the fluid flow in these devices can be achieved by using the dimensionless Reynolds number (Re) (Batchelor 2000) (Eq. 3).

$$Re = \frac{\rho v L}{\mu} \qquad \text{Eq. 3}$$

Here ρ is the mass density of the fluid, v is the characteristic flow velocity and L is the characteristic dimension (e.g., the channel width). At large Re turbulence appears while at low Re the flow is laminar. In the latter case one can imagine the liquid moving in parallel sheets of constant velocity, with no flow between the sheets. The numbers assigned to the transition between turbulent and laminar flow depend on the exact scenario, but for a pipe turbulence is present for Re>4000 and pure laminar flow is present for Re<2100 (Holman 2001). In case of microfluidics (with aqueous fluids) the Reynolds number is extremely low (usually Re<0.1) and the flow in this case is laminar. The Reynolds number describes the relation between viscous and inertial forces. At small Re viscous forces dominate and inertial effects are negligible. Therefore, after a change takes place in the flow defining parameter (*e.g.*, driving pressure) the flow changes instantaneously. This can be seen if we rewrite the Navier-Stokes equation for the low Re case. In case of a Stokes flow (Kirby 2010), *i.e.* when Re<<1 and no external forces are present some terms in Eq. 1 may be omitted and we have a simpler formula (Eq. 4):

$$0 = -\nabla p + \mu \nabla^2 v \qquad \text{Eq. 4}$$

The Stokes flow described by Eq. 4 has some remarkable characteristics. There is no explicit time dependence (except through time dependent boundary conditions), *i.e.* the flow doesn't change if the boundary conditions don't change. The changes in response to altering boundary conditions are instantaneous. Connected to time independence is time reversibility: if a particular flow satisfies Eq. 4 than the reverse flow is also a solution. Finally linearity of Eq. 4 means that the flow changes proportionally to the driving forces.

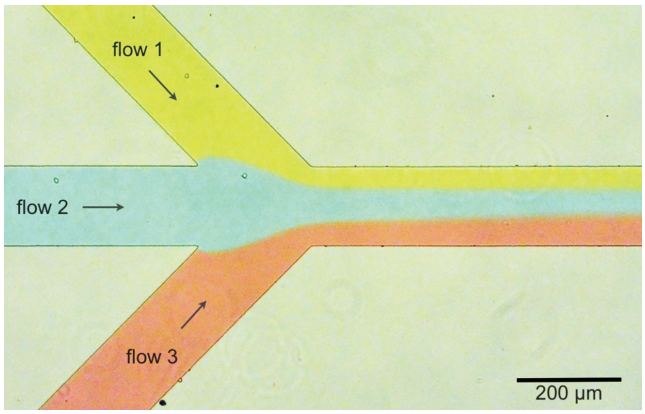

Figure 3. Flowing dye solutions in a microfluidic device. After merging the flowing solutions create a laminar structure. Smearing due to diffusive mixing can be observed at the boundaries of the layers.

These physical characteristics are important in the biological applications of microfluidics. Due to the laminar flow and the lack of turbulence mixing of fluid may take place only through diffusion (Fig. 3).

So far we omitted the effect of external forces on the fluid flow. Gravity leads to the presence of hydrostatic pressure, which is typically negligible due to the small vertical dimensions of microfluidic devices. However, by connecting external fluid reservoirs that are elevated compared to the level of the microfluidic chip, fluid flow in the device can be driven by hydrostatic pressure.

Construction of microfluidic devices

Several microfabrication methods are used for creating microfluidic chips. Some of these techniques were derived and adapted from the microelectronics industry. Therefore, photolithography and various etching methods are used to create microstructures in silicon and silicon dioxide substrates. These techniques and materials are routinely used in the production of computer chips; therefore, the methodology is well matured. These techniques however require an infrastructure that is not readily available for most research labs. Therefore, simpler and more economical fabrication processes were worked out that are now adapted widely. Soft lithography is a relatively simple and cost effective way to produce simpler microfluidic structures (Qin et al. 2010). This method is based on the creation of a master mold by photolithography and reproducing it by replica molding using polydimethylsiloxane (PDMS) (Fig. 4). First a layer of UV sensitive resin (photoresist) is spread on a substrate by spin coating. Through a lithographic mask (usually a printed transparency film or glass with a patterned chromium layer) the photoresist by UV light. The UV induces chemical reactions in the photoresist. This results the selective removal of the resin from the substrate during the development step. The remaining photoresist structure is used as a master mold for the subsequent replication process. For this liquid PDMS (typically prepared by mixing curing agent to a polymer base) is poured over the master mold. PDMS is cured by heat treatment (typically between 20-120 °C). This results the polymerization of PDMS which becomes a rubber-like flexible substance. This can be peeled off the master mold. The PDMS piece at this point contains the structure of the channels and chambers of the microfluidic design as open indentations. Access holes for small tubings can be punched in the PDMS piece for fluid inlets/outlets. The PDMS piece then may be closed off by placing it to a substrate (usually a microscope slide). Tight binding to the substrate is often done by oxygen plasma treatment.

By using small tubings the microfluidic chip may be connected to sources of samples, buffers or other liquids of need. The flow of these is typically driven by syringe pumps

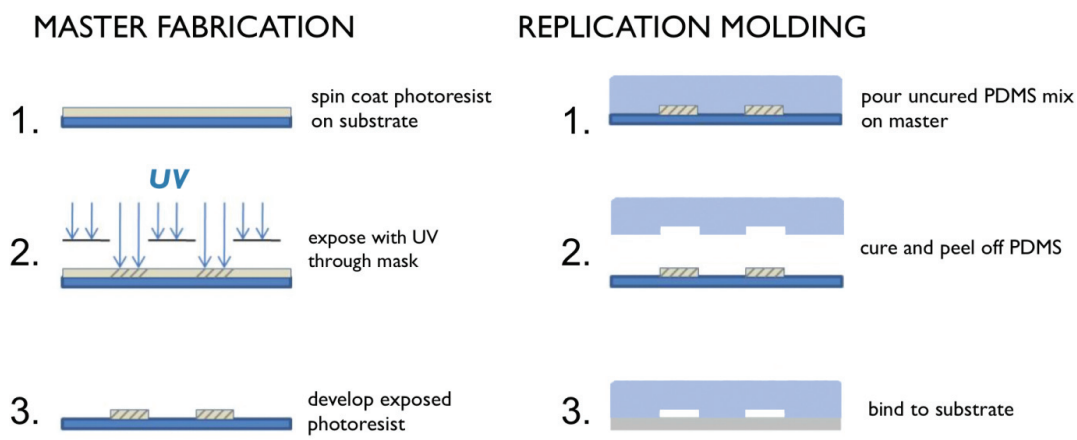

Figure 4. Step-by-step microfluidic chip fabrication by soft lithography.

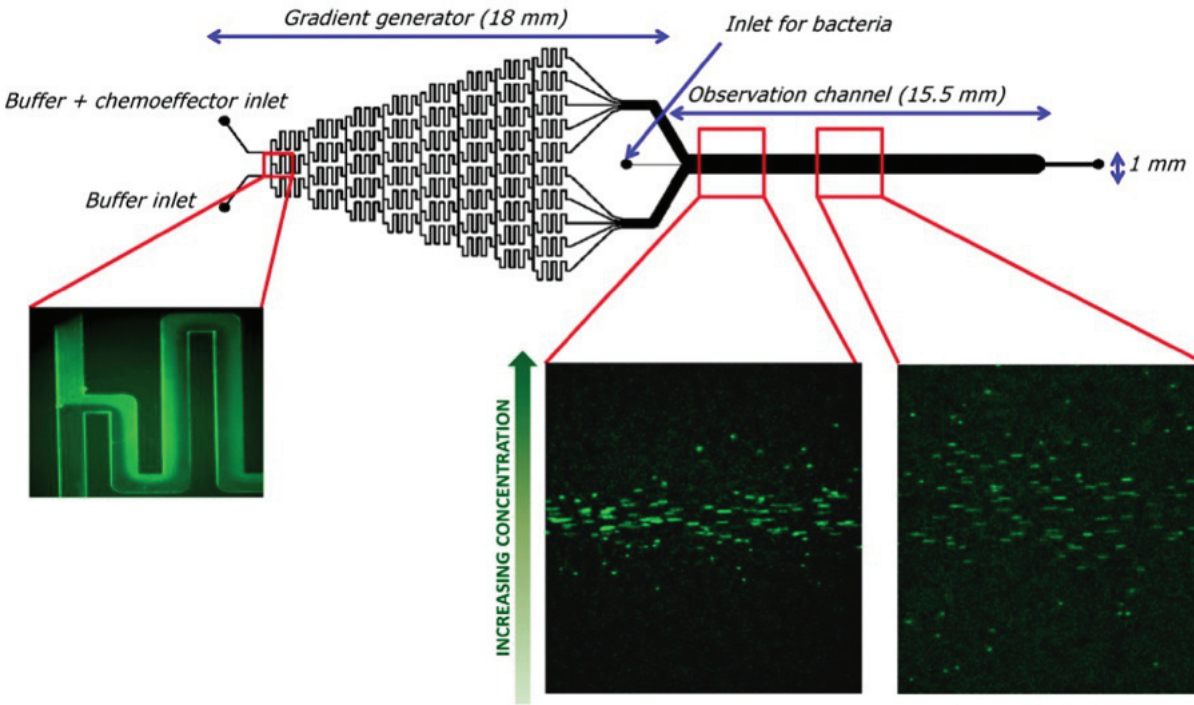

Figure 5. A microfluidic gradient generator chip based on Englert et al. (2010). In the gradient generator part diffusive mixing equilibrates the concentration distribution in split and merged narrow channels. A linear concentration gradient forms in the observation channel where bacteria are flown in a narrow stream. The distribution of the bacteria further down in the channel reflects their chemotactic response.

or various pressure sources (hydrostatic pressure in the simplest case). Various check valves and switching valves may be used in connection to the tubings to control the flow of liquids into the microfluidic chip.

PDMS is a material that is suitable for biological experiments. It is gas permeable therefore sufficient oxygen or carbon monoxide may be supplied to the cells inside the microfluidic chip by controlling the atmosphere around the device. PDMS is biocompatible and chemically resistant. It is optically clear and transparent for UV, visible and near infrared light making it suitable for various microscopy imaging techniques. Its relatively low background fluorescence makes it suitable for fluorescence microscopy in most cases.

An interesting new direction of development is the use of paper as structural material (Martinez et al. 2007; Li et al. 2012). In paper microfluidics channels are outlined by using hydrophobic materials (*e.g.*, wax). Liquid drops are placed on the suitable spots on the paper and capillary action transfers the fluid along the defined channels. Chemicals for color based reactions may be embedded in the paper at certain locations of the chip to be used for detection purposes.

Applications of microfluidics in biology

There are countless examples of how microfluidics may be used in biological research. Below is a narrow and rather personal selection of some topics that represent the diverse possibilities of this emerging technology.

Microfluidic techniques make possible the precise control of liquid flow and composition in microscopic volumes and dimensions. Numerous biological applications use this ability to accurately control the environment of biological objects such as cells and tissue cultures, and measure their response to different environmental effects.

Several ways have been worked out to create chemical concentration gradients on the microscale and study the gradient dependent chemotactic response of single cells or populations. Flow based devices create the gradient by merging two fluid inlets (with different concentrations of the chemical of interest) into a single flow channel. Mixing of the liquids takes place by diffusion and a chemical gradient form in the width of the flow channel (Mao 2003), similarly to that shown on Figure 3. Bacteria flow into the channel along with the merging liquids and chemotax along the gradient while carried by the liquid flow. At the merging point of the inlets the concentration profile in this device is more step-like instead of a linear gradient, which only forms further down along the channel. To get around this problem a different chip structure was introduced (Englert 2010). The inlets are split to narrow channels and merged in a way that in each elementary

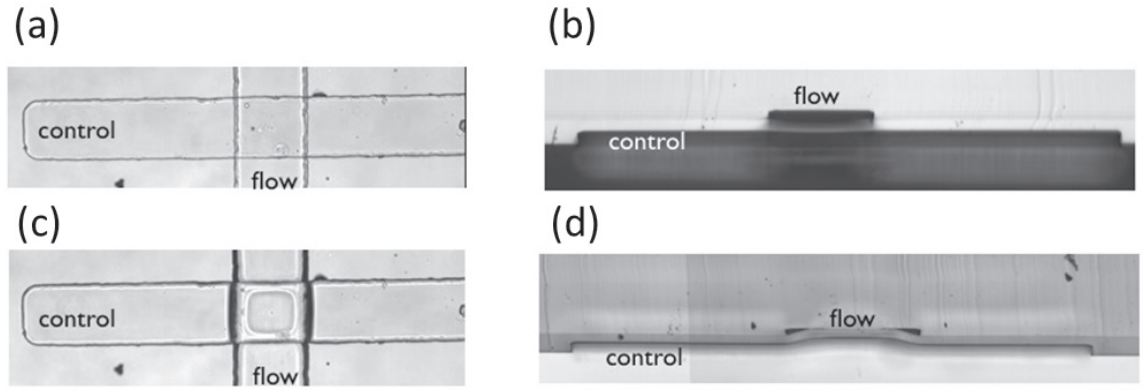

Figure 6. Pneumatically activated PDMS valve. (a) Top view of the open valve. (b) Cross sectional view of the open valve (cut through a microfluidic chip). The control channel is not pressurized, the flow channel is unobstructed. (c) Top view of the closed valve. The contact area of the PDMS membrane and the flow channel top is visible. (d) Cross sectional view of the open valve (cut through a microfluidic chip). The control channel is pressurized. The PDMS membrane is deflected and obstructing the flow channel. The flow channels in the images are 150 μm wide.

channel diffusive mixing generates a well-defined concentration (Fig. 5). When these elementary channels are unified in a larger flow channel a linear concentration profile forms in the width of the channel. Bacteria are flown in this channel in a narrow stream. While flowing along they exhibit a chemotactic behavior in response to the gradient. The distribution of cells across the width of the channel therefore reflects this chemotactic response. Due to the fluid flow (and the typical uneven flow profile in the channel) various complications emerge that make these devices less suitable for sensitive and accurate chemotaxis studies. Therefore, flow-free microfluidic chips were developed where gradients form in stationary fluid and the chemotactic effects may be studied in a greater accuracy (Diao 2006).

Microstructures provide a way to physically confine cells and study how this spatial confinement affects the cells. It has been shown for example that bacteria may get through slits with subcellular dimensions (Männik et al. 2009). Bacterial cells flatten out considerably during this process, but they are able to maintain cell division (Männik et al. 2012).

Confined space around a cell may lead to auto-induction due to cell signaling. Quorum sensing is used by bacteria to trigger and synchronize common actions. By interacting through small signaling molecules bacteria may alter their gene expression pattern in a cell density dependent manner. In an experiment by Boedicker and co-workers (2009) single *Pseudomonas aeruginosa* cells were confined in microscopic droplets created by microfluidic methods. The signaling molecules released by the individual cells remained trapped in the droplet around them. In some of the droplets the signal concentration reached a threshold and the gene expression pattern of the cell changed accordingly, just like in quorum sensing.

The appearance of active elements such as valves and pumps integrated on a microfluidic chip extended tremendously the complexity of microfluidic applications. Pneumatically activated valves are the most widespread of the integrated active elements (Fig. 6). Developed by Unger and co-workers (2000), these valves use pressure (or vacuum) to deflect a PDMS membrane to close off and open a fluidic channel. These elements make it possible to integrate and automate various tasks and processes on a single microfluidic platform. For example a chip has been developed to isolate and lyse single bacterial cells and perform PCR all on the same chip (Marcy et al. 2007). The device has been used to identify various unculturable oral bacteria.

Microfluidic chips may be used as engineered habitats for bacterial populations. Then the effect of the structure of the environment on the behavior and development of the population(s) may be studied in a well-controlled manner.

Keymer et al. (2006) used a linear array of microchambers connected with narrow channels to study the bacterial colonization of this "patchy" habitat and the development of the population structure. In the device a metapopulation (*i.e.* a system of interacting subpopulations), was formed and the bacteria showed a dynamically changing pattern of spatial distribution. With a similar device it has been shown that the patchy structure of the habitat realized by an array of coupled microchambers supports the long term survival of cooperator phenotypes when competing with cheater mutant cells (Hol et al. 2013).

The spatial structure of the habitat may deeply influence the evolution of the bacterial population. Zhang and co-workers (2011) used a microchip with a hexagonal array of chambers in which bacteria were able to move and reproduce. The antibiotics ciprofloxacin was delivered in at a certain

location, at the edge of the hexagonal chamber array. Bacteria exhibited an uneven spatial distribution in the device, and starting at certain locations in the device resistant bacteria emerged and proliferated throughout the structure. Antibiotic resistance emerged as fast as in 10 hours and from a population as small as 100 cells.

Microfluidic devices are suitable for tissue culturing too. Devices of different complexity have been constructed to study mono-cultures or co-cultures. For example Kim and co-workers (2006) used the uneven flow profile of the medium flow to study the effect of shear stress on embryonic stem cells. They have demonstrated a greater proliferation for cells grown under higher shear stress. Alternatively varying the flow channel geometry can also be used to exert different amount of shear stress on cells cultured in the device (Lu et al. 2004).

In the so-called organ-on-a-chip applications microfluidics is used to mimic certain environmental aspects of various tissues in certain organs. PDMS devices may be used for example to simulate the mechanical stress on lung tissue during breathing (Huh et al. 2010). Cells were cultured on a PDMS membrane and a pneumatic method was used to periodically stretch and relax the membrane. This cyclic mechanical strain amplified the toxic and inflammatory effect of nanoparticles. Besides lung tissue, several other tissue types were successfully cultured in microfluidic devices (Huh et al. 2012). These works pave the way towards more complex microfluidic systems that may in the future replace animal testing for drug screening.

In summary we can say that microfluidic technologies can greatly contribute to experimental research in various fields of biology and also have the potential for biomedical applications. The new methods and techniques ensure the proliferation of the routine use microfluidic devices for scientific applications.

Optical micromanipulation

Introduction

Manipulating single biological objects on the nanometer and micrometer scale has always been important in biological and medical research. Manipulation includes translocation, deformation, changing the behavior or even damaging the objects under study. In this section we introduce a range of techniques that utilizes light for such manipulative tasks. Using light for such manipulative tasks has the advantage of avoiding the introduction of "hard" equipment, such as a needle or micro capillary to the sample volume. Besides, its wavelength and power can be practically arbitrarily chosen to the actual task, keeping in mind the ranges of these parameters where damage

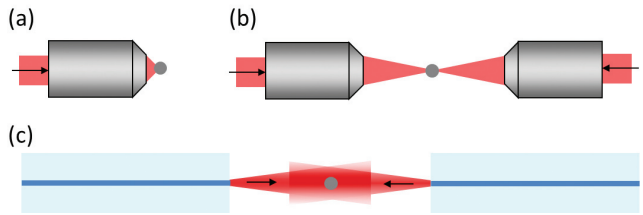

Figure 7. Schematic representations of three basic optical traps. (a) Single beam optical trap: one, high NA objective focuses the trapping laser beam. (b) Counter-propagating trap: two, low NA objectives focus the beam into one common focal position. (c) Counter-propagating fiber trap: beams emerging from two, oppositely facing single mode fibers act as a trap.

can be made on the biological sample ("opticution", Ashkin and Dziedzic 1989). In many occasions special, sometimes freely and dynamically adjustable light distributions provide extra benefit. In this section we introduce optical manipulation methods through a few examples with samples ranging from the level of DNA to the whole cell.

One of the most spectacular examples of light-matter interaction – with relevance to optical manipulation – was explained by Johannes Kepler, the astronomer of the 17th century. He hypothesized that the reason why the tails of comets always point away from the Sun is because some sort of rays originated from the Sun remove part of the comet's material and push it outward. The phenomenon was explained theoretically in the 19th century by James Maxwell. The invention of the laser had a great impact on the field, giving rise to much larger effects and more controlled experiments that could be observed before. It was in 1970 when Arthur Ashkin published his groundbreaking experiment performed on microspheres dissolved in water that were illuminated by weakly focused laser beam. He observed that the spheres are propelled forward to the direction of light propagation while attracted to the center of the beam (Ashkin 1970). In 1986 he constructed the first single beam optical trap, the version which is still used in many applications consisting a large numerical aperture (NA) objective focusing tightly a single laser beam (Ashkin et al. 1986).

Optical traps have several versions today, among which the following three arrangements are used most often (Fig. 7). The first is a single beam trap that consists of a parallel laser beam that is focused into a small focal spot by a high numerical aperture (Ashkin et al. 1986). The counter-propagating trap consists of two laser beams travelling the opposite directions and focused to a common focal spot by two microscope objectives (Ashkin 1970). In this case the objectives do not have to be of high NA. The third arrangement consist of two single mode optical fibers into which laser beams are focused at one end, and when these beams emerge on the other ends, which are facing each other at a short distance, the slightly

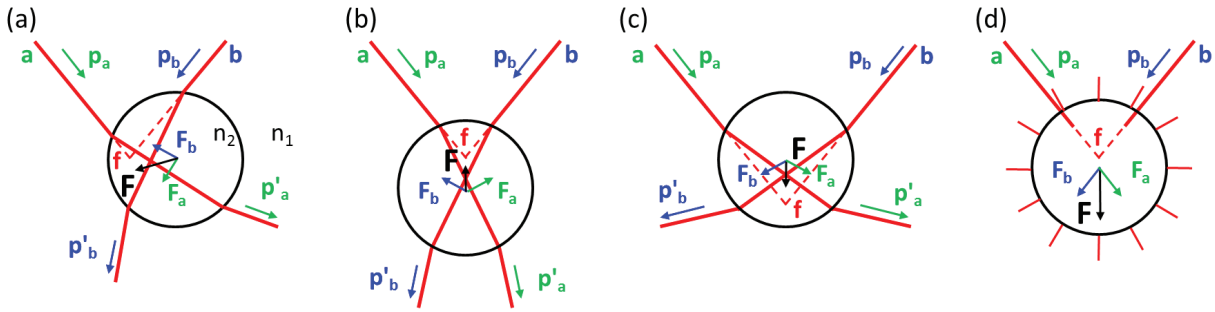

Figure 8. Origin of optical forces acting on a microbead. The figures show the deviations of the extreme rays of the focused beam in cases of (a) lateral displacement, (b) displacement below the optical axis, (c) displacement above the optical axis of the microbead and (d) the scattering of the trapping light on the bead.

diverging beams perform the trapping. Axially the balance of the radial pressure acts as a trap, perpendicularly to this direction the gradient of the optical field stabilizes the object (Constable et al. 1993; Gluck et al. 2001).

The origin of the optical force

In order to understand the origin of the force that keeps microparticles in the optical trap we have to remember that every photon that makes up the beam of the trapping laser carries the energy of

$$E = \frac{hc}{\lambda}$$

where h is the Planck constant, c is the speed of light and λ is the wavelength of the radiation. Also, every photon carries a momentum of

$$P = \frac{h}{\lambda}$$

In cases of light-matter interaction, that can be, e.g., absorption, refraction, reflection, the momentum of the photon changes. The momentum change is the consequence of a force that the matter is exerting on the photon. At the same time, the photon also exerts force on the matter with the same magnitude but with opposite direction.

The generation of the trapping forces is illustrated on Figure 8 with the single beam arrangement: the laser beam is focused by a large numerical aperture (NA) objective on a transparent sphere (refractive index: n_1) that is suspended in water (refractive index $n_2 < n_1$). The direction of the extremal beams (beam "a" and beam "b", shown on the figure) makes a large angle to the optical axis and the beams carry the momenta of p_a and p_b. Upon refraction on the sphere the beam directions change therefore new momenta p'_a and p'_b will differ from the original ones. The change of momentum means that the bead exerts force on the light, and in return light exerts forces F_a and F_b on the sphere with the net force F. Figure 8 (a-c) illustrate what happens when the sphere is moved out of the focal position sideways, downward and upward, respectively. The net forces in each three cases are such that it moves the sphere back towards the focus, *i.e.* the equilibrium position; hence, the bead is trapped. On Figure 8 (d) another important effect, the scattering force is illustrated: in this case the two beams are scattered into every directions, therefore the original momenta are lost, and the net force is pushing the bead out of the focus. For successful optical trapping the trapping forces must overcome the scattering forces.

Determination of the trapping force

The trapping force can be calculated in different ways for different particle diameters. For spheres much larger than the wavelength of the trapping laser (>5 μm), the conditions for Mie scattering are satisfied, and the trapping force can be calculated with ray optics. For spheres much smaller than the wavelength of the laser (<100 nm), Raleigh scattering takes place and the trapping force can be calculated by treating the particle as a point dipole. Most often the size of the trapped objects is in between, making force calculations quite complicated. The scattering force is proportional to the trapping laser intensity, while the trapping force is proportional to its gradient. Therefore the force that pulls the trapped objects back to their equilibrium position is often called gradient force. The trapping forces can reach even a few hundreds of piconewtons (pN). Table 1 illustrates some typical forces found in chemistry and biology.

As we saw, if we move a trapped object out of the focus, *i.e.* the equilibrium position, force acts on it. This force for short displacements is proportional to the displacement itself (Hooke's law), just like in case of a spring: $F_r = -k \Delta x$, where F_r is the restoring force, Δx is the displacement and k is the factor that determines the strength of the trap: the trap stiffness. Due to this intimate relation between displacement and

Table 1. A few typical forces found in chemistry and biology.

Type of force	Example	Rupture force
Breaking a covalent bond	C-C	~ 1600 pN
Breaking a non-covalent bond	Biotin-streptavidin	~ 160 pN
Breaking weak bond	H-bond	~ 4 pN
Stretching	dsDNA to 50% extension	0.1 pN
Developed by a molecular motor	Kinesin walking on micro-tubule	5 pN

trapping force, the trapping force measurements are very often position measurements. In order to get an exact value of the force, the trap stiffness has to be also determined. Several stiffness determination methods exist in the literature, each requires the position determination of a test bead. The power spectrum method relies on the Fourier transform of the position fluctuation of the trapped bead. This method provides high precision, it is reliable and it can diagnose misalignments in the optical system but requires measurement with high bandwidth. With the method of equipartition the variance of the fluctuation of the trapped bead is calculated and used to determine trap stiffness with the following formula:

$$\frac{1}{2}k_B T = \frac{1}{2}k < x^2 >$$

where k_B is the Boltzmann constant, T is the temperature and $< x^2 >$ is the variance of the bead displacement. The trap stiffness can be determined directly by measuring the displacement of a trapped bead in response to viscous forces produced by the surrounding medium. The movement of the medium can be generated by moving the sample stage along one dimension in a triangle wave or with a sinusoidal pattern. In this case the displacement is the result of the viscous drag acting on the bead by the medium. The stiffness is calculated from the phase delay between the bead and stage positions.

Optical traps can operate in vacuum, in atmospheric pressure gas or in liquid resulting in several important results in a very wide range of topics. In vacuum, cooling of a microbead to a temperature of 1.5 mK towards the quantum mechanical ground state in its center-of-mass motion enables researchers to study several quantum effects, such as gravitational states, non-Newtonian gravity forces at small scales or even to measure the impact of a single air molecule (Li et al. 2011). Viscosity measurements were carried out by following the time course of shape oscillations of a liquid particle made by the coalescence of two particles held by optical tweezers in atmospheric pressure (Power and Ried 2014). Droplet coalescence is also of interest in processes that use dense aerosol sprays such as inhalers for drug delivery in conditions such as asthma or hay fever (Mistry et al. 2012). Examples for traps working in liquid will be presented later.

As it was mentioned earlier, the trapping is achieved via focusing a laser beam into the object to be trapped. If this object is a cell, the high intensity in the focus can easily damage it. The careful choice of the trapping laser wavelength can help avoid this problem. A near infrared light source is used most often since in the visible range (400 nm < λ < 700 nm) some cell organelles, such as chloroplasts may absorb, and in the mid infrared (2000 nm < λ) water absorption increases significantly. Trapping laser illumination reduces the cloning efficiency for instance for Chinese Hamster Ovary (CHO) cells in a very wavelength-selective way with the optimum being at 850 nm and 980 nm (Liang et al. 1996).

Applications of optical trap

Biological macromolecules

Optical trap has been being successfully used for more than two decades to study biological macromolecules from several aspects, such as mechanical properties, function or spectral characteristics. The molecules included but are not limited to myosin (Shepherd et al. 1990), kinesin (Svoboda et al. 1993), DNA (Perkins et al. 1994), RNA (Liphardt et al. 2001); even the viral package of dsDNA could be characterized with optical trapping methods (Smith et al. 2001). Due to the nanometric dimensions however, their trapping can only be facilitated indirectly, by using at least a few hundreds of nanometer-sized structures as handles. The high degree of optimization of such optical systems enables the measurement of displacements down to the sub-nanometer ($<10^{-9}$ m) or forces down to the femtonewton (10^{-12} m) regime. For instance, displacement of such small level was measured in the case of RNA polymerase (RNAP) which moves progressively along a template DNA and creates a complementary RNA on the way. In the work of Abbondanzieri and co-workers (2005) the stepwise motion of RNAP, as proposed earlier, was measured with an ultra-stable optical trapping system holding two functionalized beads (Fig. 9). During the experiments two beads were trapped in the system: the first was coated with DNA strands and was trapped strongly while the second bead was coated with the RNAP and it was trapped weakly. In the second trap the displacement of the bead from the trap center was set such that the restoring force was constant over a 50 nm region. This way the RNAP functioned under a constant load, and during its operation it "pulled" the DNA and consequently the bead in the weak trap closer to the one held by the strong trap. This step-by-step displacement was registered in the motion of the bead in the weak trap. The method provided 3.7±0.6 Å step size, which is consistent with the crystallographic spacing between neighboring base pairs in B-DNA (3.4±0.5 Å). In summary, the researchers could directly determine that the

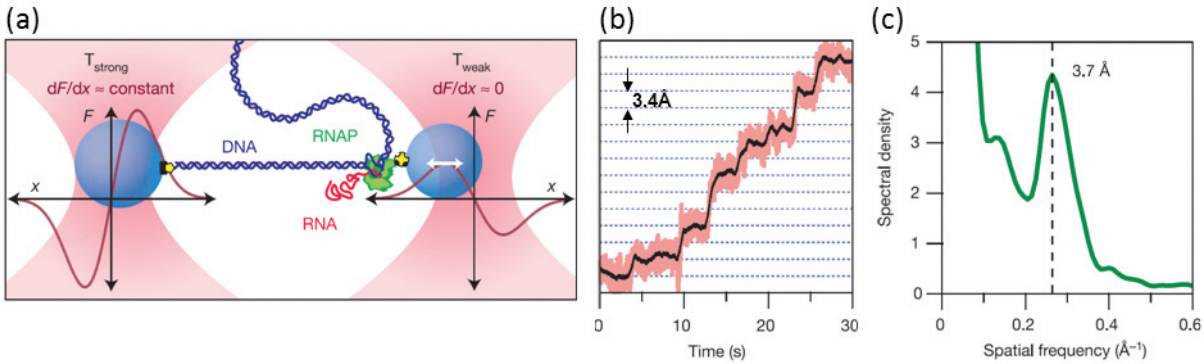

Figure 9. Measurement of the step-size of the RNAP on a DNA molecule. The experimental scheme (a) shows the stronger (left) and weaker (right) optical traps and the arrangement of the molecules. (b) Typical record for single molecules of RNAP transcribing under 18 pN load. Data is filtered with 50 ms (pink) and 750 ms (black) median filters. (c) The power spectrum of the processed record on (b) showing a peak at the dominant fundamental step size, 3.7 ± 0.6 Å. Reprinted by permission from Abbondanzieri et al. (2005). Copyright: Macmillan Publishers Ltd. (2005).

RNA polymerase takes single-base-pair steps.

Mechanical characteristics of DNA itself can also be deduced from measurements made by optical traps. Oroszi et al. (2006) used a single beam optical trap to measure directly the torsional modulus of a double-stranded DNA molecule, that links the twist of the molecule and the applied torque to achieve this twist. In their experiment they took advantage of the fact that when the trapping laser beam is polarized, a micrometer-sized trapped disk orient itself along the polarization direction and an orientational trap is formed. Thus, if the polarization direction is rotated, the disk follows its rotation. The researchers bound one end of a dsDNA to the bottom of the microfluidic channel in which the experiment was performed, the other end to a flat disk trapped by a polarized beam and stretched the DNA to the 0.5 and 0.75 of its total length. This way, when the disk was rotated by the polarized trap, the DNA strand was twisted. The researchers have found torsional modulus value of 420±43 pN nm^2 that is in good agreement with other, indirect torsional measurements. The presented method can also be used in general to calculate the torsional stiffness of any polymer.

Cell manipulation

When using optical traps on the cellular level, one very exciting field is the micro-manipulation inside cells: the targets this time are the cell organelles. As long as their refractive index is larger than that of the surrounding medium, these structures can be trapped directly unlike the macromolecules in the previous section. A nice example for the application of trapped cell organelles comes from Bertseva et al. (2012). They determined the viscoelastic moduli of the interior of two types of cells (non-cancerous human urothelial cells (HCV29) and cancerous T24 human epithelial cell lines) by monitoring the fluctuation of trapped lipid granules inside the cells. The viscoelastic modulus G'(ω) describes the elasticity of the medium and the modulus G''(ω) describes its viscosity, both in a frequency-dependent manner. In the spatial confinement of the optical trap the granules can move only in a limited distance, described by the mean square displacement (MSD). The time evolution of this quantity can be fitted by an equation containing the trap stiffness k and the coefficient that is in intimate connection to the viscoelastic moduli of the cell interior. Outside of the cell (in water) $\alpha = 1$, but inside it is around 0.75. The researchers concluded that in terms of both G'(ω) and G''(ω) the difference between the cell lines is insignificant within the experimental error, which suggests that the cytoskeleton polymer networks have similar structure.

Further expanding the range of targets, whole cells can be trapped or manipulated optically. In a recent review of Zhang and Liu (2008) a series of examples are shown to transport, sort, dissect or guide cells with light. Positioning of cells is important when spatial stability is required for instance, for localized spectroscopic measurements (*e.g.*, Raman, fluorescence). Optical traps can also relocate single cells in the medium without physical contact, which is highly desirable for working in sterile conditions. Sorting of cells by optical means cannot compete with FACS machines in terms of throughput, but when only a small number of cell is available in a few microliter solution, such systems can come handy. When optical trap is used to assemble cells, phenomena, like bacterial infection can be studied: Akselrod et al. (2006) formed a group of *P. aeruginosa* bacteria around Swiss 3T3 fibroblast for controlled colonization. Transient permeabilization of cell membranes by short laser pulses allows cellular fusion or molecular injection (opto-injection). In the work of Rao and co-workers (2009) Raman spectroscopy was used to monitor changes in the oxygenation state of human red

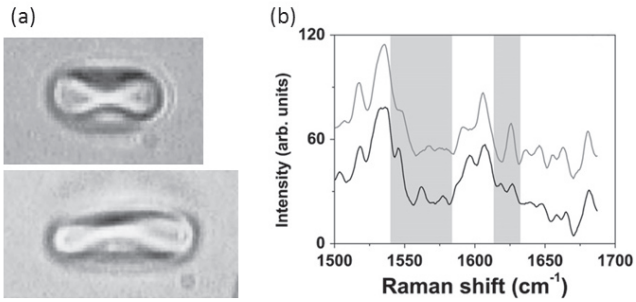

Figure 10. Raman spectroscopy on optically stretched red blood cells. (a) Optical microscopic images of a relaxed (upper) and a stretched (lower) red blood cell in the optical trap. (b) Raman spectra of a relaxed (upper) and stretched (lower) red blood cell. The shaded spectral ranges changed consistently between the relaxed and the stretched state from sample to sample. Reprinted by permission from Rao et al. (2009). Copyright: Elsevier (2009).

blood cells while they were stretched with optical tweezers (Fig. 10). This physical stress simulated the deformation that cells experience as they pass through microcapillaries. The molecular consequences of the deformation were detected on the amplitude change of specific protein Raman bands. One of the most consistent changes was observed on the 1625 cm^{-1} band, which has already been associated with the polyporphyrin side chain. The observed reduction of the band in the stretched state, which was observed previously between oxy and deoxy RBCs, is caused by the dissociation of oxygen, when the planar porphyrin structure deforms out of plane. The researchers therefore concluded that cells with a significant oxygen concentration were pushed to a deoxy state due to mechanical deformation.

The combination of fluorescent confocal microscopy and optical tweezers provide a unique combination for non-invasive manipulation and observation in studying individual cell-cell interactions. Tam and co-workers (2010) combined a spinning disk confocal microscope with an optical tweezers to trap the pathogen *Aspergillus fumigatus* and to move it to the proximity of mouse leukaemic monocyte macrophages (RAW 264.7) and studied the precise time course of phagocytosis. Positioning the fungal particle close to the macrophage and observing the events with time-lapse imaging revealed that the entire process while the *A. fumigatus* is fully enveloped within the RAW cell, took about 3.5 minutes. With 3D volumetric rendering provided by the confocal setup it was possible to confirm that the uptake of *A. fumigatus* was complete. The crucial role of the optical trap in this case was to position the pathogen to an exact distance and position relative to the macrophage.

Apart from helping the study or observation of cells, their growth can also be manipulated optically. Neuronal cell growth involves the progress of filopodia along various directions. However, controlled growth direction would be a major advancement in the research of the regeneration of damaged neurons. Carnegie et al. (2008) used linear optical traps to induce filopodia growth into pre-defined directions. The leading edge of the cell was illuminated by the linear beam, and within minutes, growth cones were observed to change direction from their initial trajectory to line up with the beam. They explained the phenomena with purely optical reasons. In their model each filopodium is made up of 20-30 actin filaments that are characterized by the sum of the polarizability of each G actin monomer. This allows the calculation of the torque acting on each filopodium when illuminated by the linear-shaped beam. Calculations showed that there are always stable positions for the filopodium in the line trap characterized by zero torque. In these positions the main axis of the line trap is almost parallel to that of the filopodium. This means that the line trap is acting on the filopodia with a few pN·nm torque that aligns them along its main axis until an equilibrium position is reached. And since filopodia alignment can be a precursor to direct growth, the direction of the trap could determine the growth direction.

Optical traps using complex microstructures

Optical tweezers can further facilitate biological research by using complex 3D structures made specifically for a special task. We already saw how simple microbeads can facilitate the use of optical trap on biological macromolecules. Trapped complex 3D microstructures can be used as microtools to probe biological objects without being bound to them (Phillips et al. 2012a), or similarly to beads, can bind them and enable indirect manipulation schemes with 6 degrees of freedom. Two-photon polymerization is a technique that is capable to produce such micrometer-scaled structures with nanometer precision (Kawata et al. 2001) that can be trapped and manipulated by optical means (Phillips et al. 2012b; DiLeonardo et al. 2012). Palima and co-workers created a microtool that is essentially a movable light guide that can be maneuvered to any position within the sample volume (Fig. 11a) (Palima et al. 2012). Most importantly, light can be coupled into the light guide at one end, and after being redirected by 90 degrees and emitted at the other end it illuminates any targeted object. Targeted fluorescence excitation localized to individual 3 μm diameter fluorescent beads was demonstrated with the tool in a microscope (Fig. 11b). The excitation was achieved along a direction perpendicular to the optical axis; illumination from this direction is not possible with a conventional fluorescence microscope. The tool is also capable of collecting emitted light from any direction perpendicular to the optical axis and directing it towards the observer. Such a maneuverable light source/probe together with fluorescent labeling of individual cells enables such special cell studies that require localized excitation from off-axis directions.

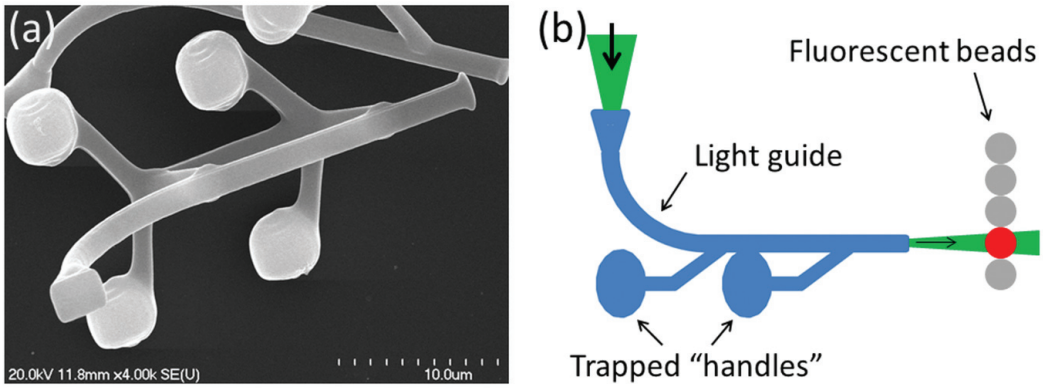

Figure 11. Optically maneuvered mobile light guide. The scanning electron micrograph (a) shows the four spherical parts through which the tools can be trapped and the curved light guide part (radius of curvature: 5.8 μm) that redirects the fluorescence excitation (top view). (b) The tool was trapped by the "handles" and its tip was directed towards the fluorescent microbeads. The green excitation light was coupled in at the top and it emerged from the tip illuminating the selected bead; only that bead was observed emitting light.

Atomic Force Microscopy

Theoretical background

The advent of optical microscopes has opened a window into the micro-world, besides imaging, by facilitating and conducting the direct "touching" and "manipulation" of micro-scale objects. The extension of this field, beyond the optical limit, towards nano and pico scales supported the development of several micromanipulation techniques. Combination of high resolution imaging and nano-force testing gave birth to the one of the most versatile and powerful tools in micromanipulation: the Atomic Force Microscope (AFM). As a member of the Scanning Probe Microscope (SPM) super family, it was invented in the early eighties by Gerd Binning and his co-workers (Binnig et al. 1986). At that time Binnig and Heinrich Rohrer, was awarded with Nobel Prize "for their design of the scanning tunneling microscope", which was the precursor of the AFM.

The technology incorporated by the AFM, opened large avenues for *in vitro* biological applications concerning fields from single molecule imaging to cellular mechanics and morphology. As it can operate in liquid environment and at human body temperature, it became the most reliable and accurate nanoforce-tool in the research of cell biophysics.

Key features of the Atomic Force Microscope

Briefly, the AFM detects inter-atomic forces, which explains the term 'atomic'. To achieve this, a very sharp needle is brought into contact with the sample to be investigated. At the theoretical edge, a single atom of the tip interacts with a single atom of the sample. As Figure 12 depicts, at the heart of every AFM resides this sharp tip, which is situated at the end of a soft and a relatively long cantilever. The force resolution of the system, defined by the cantilever's spring constant and the thermal noise, is in the range of few piconewtons. Beyond this range, special cantilevers and stable environmental control are needed which mostly excludes the investigation of biological objects.

Depending on the requirements of the field in which they are applied, the cantilever and the tip are usually made of a large variety of materials: silicon, tungsten, platinum/iridium, silicon nitride, carbon or gold, just to name a few. Tip shape and cantilever stiffness can be chosen accordingly to experimental setup; from ultra-sharp to micron sized colloidal probes, from extra soft to high rigidity and conductivity cantilevers. The palette is quite large with almost unlimited possibilities if we take into account that tip decoration with functional molecules enlarges the variety, resulting highly accurate and versatile nano-probes.

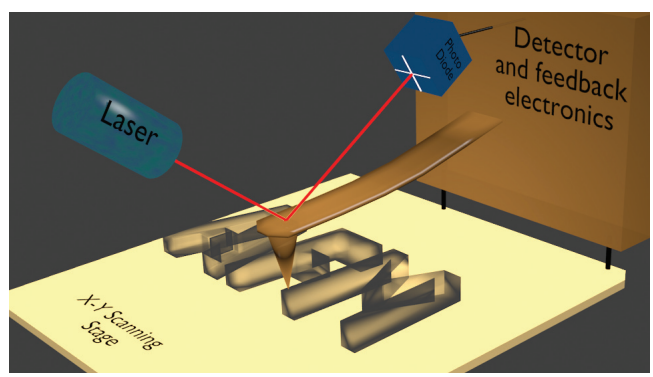

Figure 12. Schematic representation of key components and basic operation of the Atomic Force Microscope.

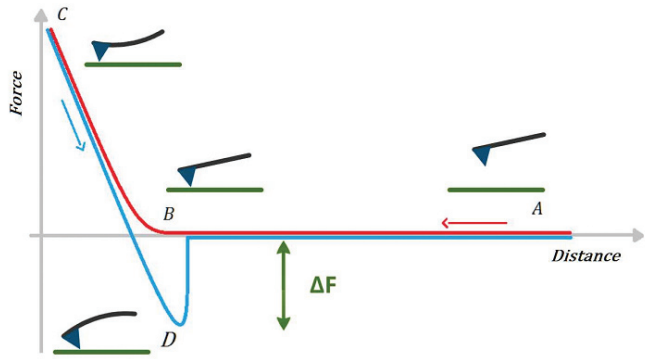

Figure 13. Schematic diagram of a force curve. Characteristic steps of a force-distance curve: lowering the tip to the sample (A), direct contact point with the sample (B), reaching the maximal vertical deflection of the cantilever (C), maximal downward cantilever deflection (D). Red is assigned to lowering, while blue line represents the pulling back of the cantilever.

Deflection of the cantilever upon tip-sample interaction has to be detected and recorded accurately. Several methods were tested during the early stages of AFM development, nowadays the most common is one of the optical methods, due to its simplicity, versatility and low cost. Basically, a narrow infrared laser beam is reflected from the backside of the tip-holding cantilever, and its pointing position is detected by a photodiode. Upon splitting the photodetector into four segments, deflections and torsional motions of the cantilever can be differentiated (Fig. 12).

Shorter cantilevers offer larger angular displacement of the laser beam; however the sensitivity is limited by random thermal noise (Meyer and Amer 1988). Vertically sub-nanometer resolution can be easily achieved, while horizontally the tip-sample convolution is needed to be taken into consideration at final analysis.

High resolution imaging

Recording topography requires accurate three-dimensional positioning. Accordingly, the scanning mechanism provides free displacements for all three dimensions of space. High accuracy and reproducibility has led to wide spreading of piezoelectric transducers. As the tip moves along the surface of the sample, interacting forces acting on the probe are recorded line by line, point by point. Acquisition of one image, depending on resolution and scanning rate applied, is at the order of few minutes. Video rate AFM is available on the market (Picco et al. 2007; Ando et al. 2008), but due to its special sample preparation and limited scan size it is less used in life sciences. On the other hand, combination with other techniques provides considerable improvements of simultaneous investigations (Deckert-Gaudig and Deckert 2011; Kellermayer 2011).

Basically two different imaging modes can be distinguished: "Contact" and "Alternate Contact" (AC) mode (found as tapping-mode in some cases). During raster scan, in "Contact mode", the deflection of the cantilever is kept constant by a feedback loop. In "AC mode", the cantilever oscillates at or near its resonant frequency and the feedback loop minimizes the amplitude deviations. As three-dimensional topography is recorded during scans, no subsequent data processing is required to reconstruct three dimensional images.

Non-invasive, sub-nanometer resolution imaging in liquid at human body temperature, puts the AFM at the leading front of biophysical investigations of biomaterials. It is suitable for applications at large scale range, from living cells (Bálint et al. 2007a) through membranes (Végh et al. 2011a) down to single molecules (Gad et al. 1997; Rief et al. 1997), covering over four orders of magnitude. Molecular imaging made a large advancement in 2013, when de Oteyza and his colleagues captured covalent bonds before and after a complex reaction (de Oteyza et al. 2013).

Force Spectroscopy

Besides non-invasive and high resolution imaging, the AFM provides invaluable data as a nanomechanical tester, even simultaneously in many cases. Starting from single molecule spectroscopy, through membrane dynamics up to cellular level studies, it represents a powerful technology for *in vitro* micromanipulation experiments. Among its many interesting features, such as friction measurement (Coles et al. 2008), microlithography (Davis et al. 2003) etc., acquisition of force-distance curves, is outstanding. As an accurate nanomechanical tester, offers wide range of possibilities in living cell biophysics (Bálint et al. 2007a; Carl and Schillers 2008; Franz and Puech 2008).

Force curves can be achieved simply by lowering (trace) the probe onto the sample, until a pre-defined bending of the cantilever is reached, and pulling back (retrace) to initial position. The basic force curve holds the force acting on the cantilever vs. its vertically travelled distance (Fig. 13). Based on these curves, many useful parameters can be calculated, but their holistic enumeration points beyond the limits of this study. Only those most relevant to cell biophysics are discussed hereby.

The most widespread and employed parameter as a measure of stiffness is the tensile or elastic modulus. Based on Hooke's theorem, this parameter quantifies the ability of a given material to withstand stress. By recording a usual force-distance curve, the sample's tensile or Young's Modulus (YM) can be calculated (Vinckier and Semenza 1998). On the Figure 13, point B marks the probe-sample contact. Values recorded between this point and maximum force (point C, Fig. 13) are necessary to calculate the tensile modulus.

As a reference, the cantilever's own deflection needs to be eliminated, simply by subtracting a force curve recorded on hard surface, *e.g.*, Petri dish. The obtained force-indentation curve between contact point and maximal force point, gives the sample's elastic modulus.

Another important parameter is the maximal adhesion force, denoted with ΔF on Figure 13. Regardless of its origin, real time probe–sample adhesion can be monitored with high accuracy (Benoit and Selhuber-Unkel 2011). As biochemical and biophysical signaling of living cells relies on protein-protein interactions, protein functionalized probe – cell surface adhesion is an *in vitro* technique to test receptor-binding forces with AFM. It consists of applying a constant and controlled force to a receptor-ligand bond. As a result, dissociation lifetime can be calculated (Yuan et al. 2000; Wojcikiewicz et al. 2006; Robert et al. 2008).

In reality, none of the materials behave purely as Hooke's law predicts. Both viscous-like and elastic characteristic are present upon mechanical strain. The manner how a material relieves stress under constant strain is described by stress relaxation. AFM is a good candidate to detect relaxation of various materials, *e.g.*, living cells. Furthermore, taking a force-distance curve in each defined point of an imaging area, elastic (or adhesive) maps can be reconstructed. Recording simultaneously the topography and elastic properties are absolute advantage of the AFM.

Applications of AFM

From single molecule topography to membrane protein mapping

Studies of membrane proteins based on cryo-electron microscopy and X-ray crystallography resulted important data about their structure and molecular architecture. However, heterogeneity, solubilization problems and size of protein complexes might induce difficulties in their structural investigation (Lacapere et al. 2007). AFM may provide valuable information about membrane proteins at single molecule level, near physiological conditions (Muller 2008). For a detailed review on single molecule force spectroscopy see the review of Kedrov and co-workers (2007).

There are many human disease associated with protein aggregation and accumulation, among which the number of those related to amyloid or amyloid-like aggregates' deposition is over forty (Chiti and Dobson 2006). Three dimensional nanometer-scale images of ex-vivo amyloid fibrils and pre-fibrillar aggregates taken with AFMs play an important role in their morphological characterization (Chamberlain et al. 2000).

One of the most abundant connective tissue protein in mammals is collagen, hence its proper formation and function is crucial. High-resolution in vitro topographs of self-assembled collagen fibrils might help to understand and describe formation of those in vivo. Recording sequential time-lapse tapping-mode AFM images on collagen fibrils, Cisneros and his coworkers observed lateral and longitudinal fusion of single fibrils (Cisneros et al. 2006). Moreover, they have proved that the AFM can cope with or even substitute the electron microscope, due to its high resolution, the ability to record the dynamics of functional biomolecules and the great potential of various biotechnological and biomedical applications.

Nevertheless, there are studies which do not follow the conventional AFM methods (*e.g.*, imaging, force spectroscopy, micromanipulation). One such is the direct measurement of protein motion upon the conformational change of the incorporated retinal protein. Simply by adsorbing oriented purple membrane fragments onto the tip-side surface of an AFM cantilever and recording its deflection when illuminated, the motion of single molecules can be estimated (Bálint et al. 2007b).

Receptor-ligand interactions

Entire organisms are controlled and regulated by a large variety of interactions between biomolecules. The process when a biomolecule attracts another in its close proximity and then binds to it is called bio-recognition (Bizzarri and Cannistraro 2010). By these specific recognition mechanisms, biomolecules can build reversible or irreversible complexes, which are able to perform countless number of functions (*e.g.*, during cell adhesion, cell movement, cell shape development, environment recognition, in the genome replication and transcription, signaling, immune-responses). The binding strength between these molecule pairs fall in the range of nanonewton-scale forces. For the direct measurement of these tiny force values, one of the most effective tools is the AFM. Chemically attaching the receptor protein to a supporting surface and the ligand to the end of a tip, results a direct nanoforce receptor-ligand binding tester. By analyzing the magnitude of the binding forces depending on the withdrawal speed, which is a recognized method in the literature, the characteristic parameters of the interaction can be determined. The first direct measurements of receptor-ligand unbinding forces by AFM date back to mid-nineties. Florin and his coworkers were pioneers of this field, when they quantified the binding force between avidin and biotin, desthiobiotin and iminobiotin using atomic force spectroscopy (Florin et al. 1994; Moy et al. 1994). Ever since, the Single Molecule Force Spectroscopy became widespread and has evolved into a cutting edge technology in the frontline of the bio (molecular) physics.

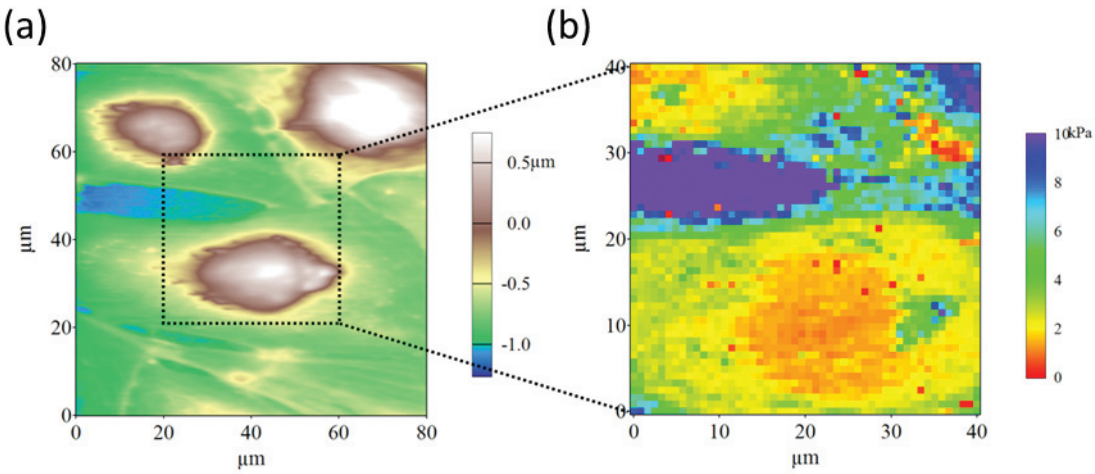

Figure 14. Height and elasticity maps on living cells. (a) Height image of confluent human brain endothelial hCMEC/D3 cell line layer. (b) 50 by 50 points elastic map recorded on the area marked on panel (a).

Cellular biomechanics

From the dynamic pushing and pulling during tissue development, cells in their native environment are subjected to constant processing of mechanical signals, implying continuous control on morphology and adhesion. Cellular morphology is strongly related to survival and reproduction ability too; therefore, any alteration might be fatal (Iyer et al. 2009). Consequently, cell motility is determined by connections between cytoskeleton and intercellular junctions as well as by interacting molecules with the extracellular matrix. Multicellular organisms rely on proper adhesion between individual cells and interconnecting tissue. Binding to a surface or to another cell may be crucial even for unicellular organisms (Ubbink and Schar-Zammaretti 2005; Zhang et al. 2011).

Structure and cellular micro- or nanomechanical properties are strongly interconnected. Their understanding is essential to improve treatment of pathologies. Stiffness alterations of blood-travelling cells might have pathological consequences; however, it is difficult to measure their elasticity, due to their mobile nature. Nevertheless, interesting ways for immobilization and measurements were introduced in their research (Dulinska et al. 2006).

Erythrocytes (red blood cells, RBC) are common type of vertebrate's blood cells. Their structural and functional alteration can manifest in vast range of dysfunctions and diseases. AFM is a powerful method to investigate RBC's morphology, physical parameters and biological properties under near-physiological conditions (Dulinska et al. 2006). Many diseases concerning the heart and the circulatory system were linked to insufficient deformability of RBC's (Starzyk et al. 1999).

Elastic properties of surface adherent cells are mostly determined by cytoskeletal and membrane components (Kumar and LeDuc 2009). Cytoskeletal polymer organization and membrane fluidity are the most important components, which determine cell morphology and elasticity. High resolution topographies may not reveal only morphology, but even cortical cytoskeletal organization as it can be seen on Figure 14a. Elastic map is reconstructed from 50 by 50 force curves taken at the marked area (Fig. 14b). This technique is widely used for cell biomechanics investigations, examples *e.g.*, neuronal growth cones (Martin et al. 2013), endothelial cells (Végh et al. 2011b), tumor cells (Moreno-Flores et al. 2010). The effect of drugs on cell stiffness, *e.g.*, targeting cytoskeletal remodeling or membrane fluidity, can be studied successfully using AFM based elastic maps.

Measuring direct cell-cell interaction

With no concern of completeness, here are some interesting and exciting studies where the atomic force microscope was involved as a nano-force tool in order to investigate intercellular connection strength.

One of the most common bacterial infections concerns the urinary tract, affecting millions of people worldwide (Foxman et al. 2007). Uropathogenic strains of *Escherichia coli* bacteria are among the leaders responsible for urinary tract infections. The usual management includes long term antibiotics; however considerable resistance cannot be neglected (Cetin et al. 2009). Proper adhesion of bacteria to uroepithelial cells is a crucial step towards infection. Yatao Liu and his co- workers (2010) used an interesting and straightforward AFM based method to investigate direct bacterial-uroepithelial cell adhe-

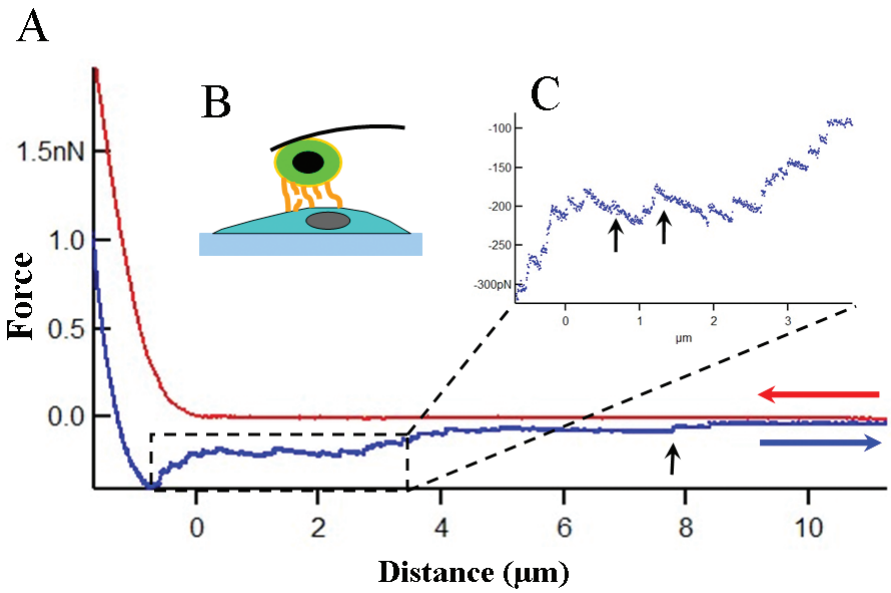

Figure 15. Hallmark of inter-cellular bonds. (A) Force-distance curve recorded with a tumor cell decorated tipless cantilever on a confluent layer of endothelial cells. (B) Schematic representation of the measurement setup: green marks the tumor cell on the cantilever while the endothelial cell on the surface is blue. Yellow stripes represent the membrane tubes pulled out of cells. (C) Magnification of the marked zone from the panel A retrace curve.

sion in presence of red cranberry juice cocktail. Simply immobilizing a bacterium at the end of an AFM tip, they have proven that red cranberry juice reduces the adhesion force between the bacteria-decorated probe and a confluent layer of uroepithelial cells.

Towards understanding and description of cancer and metastasis formation, mechanical investigations have recently gained enlarged interest (Suresh 2007). More and more results underline the lack of stiffness in cancerous cells compared to normal tissue cells where they originate from (Cross et al. 2007; Li et al. 2008). Metastasizing cells alter their shape and adhesion in order to be able to travel along the organism to form new colonies far from primary tumors. Their biomechanical properties undergo certain change in order to sustain non-controlled development and survival (Kumar and Weaver 2009). While the division rate of these cells is higher, their biomechanical properties need to go through dramatic adjustments.

Brain metastases are among the most feared complications of cancer because they often cause profound life impairing neurological symptoms (Norden et al. 2005). Additionally, lung cancer and melanoma have a greater tendency to form multiple metastases (Shaffrey et al. 2004). Presence of brain metastasis is of very poor prognosis; the median survival time can be counted in months, rarely few years. Metastasis formation in remote organs requires blood or lymphatic transport of cancer cells. Since the central nervous system (CNS) lacks lymphatic circulation, the blood stream is the single option. However, metastatic cells invading the CNS do need to cross the blood-brain barrier (BBB). The vascular endothelial cells with outstanding characteristics play important role in the process of transmigration, as the endothelial lining is the first obstacle encountered by extravasating cancer cells. A simple model which includes immobilization of a cancer cell to a tipless AFM cantilever and a layer of brain endothelial cells could provide important information regarding their bond formation dynamics (Végh et al. 2012). Fig. 15 shows a typical force-distance curve recorded between a tumor and an endothelial cell (Fig. 15, panel A), the schematic arrangement of such measurement (Fig. 15, inset B) and an interesting feature of these curves (Fig. 15, inset C). Namely, the connection between the two cells is breaking up in discrete steps, in some cases even microns away from contact point (Fig. 15, point B). This underlines the theory that individual membrane tubes are pulled out of cells. These are membrane 'tethers' (marked with yellow on Fig. 15, inset B), that might help in the establishment of firm adhesion. Similar process was described by Sundd and his coworkers in case of leukocyte rolling at high shear stress (Sundd et al. 2013).

Investigation of the adhesion between a metastatic cancer cell and a confluent layer of brain endothelial cells might lead to alternative ways of prevention and treatments. Deeper insight into mechanical properties of cancer cells, and their interactions during invasion, offers better understanding of

morphology and nanomechanics related processes. Even more, opens the way to new developments in cancer diagnostics, therapeutics and drug efficacy.

Acknowledgements

This work was supported by the TÁMOP-4.1.1.C-13/1/KONV-2014-0001 program entitled „Practice-oriented, student-friendly modernization of the biomedical education for strengthening the international competitiveness of the rural Hungarian universities".

References

Acheson DJ (1990) Elementary Fluid Dynamics. Oxford Applied Mathematics and Computing Science Series, Oxford University Press, Oxford.

Abbondanzieri EA, Greenleaf WJ, Shaevitz JW, Landick R, Block SM (2005) Direct observation of base-pair stepping by RNA polymerase. Nature 438:460-465.

Akselrod GM, Timp W, Mirsaidov U, Zhao Q, Li C, Timp K, Matsudaira P, Timp G (2006) Laser-guided assembly of heterotypic three-dimensional living cell microarrays. Biophys J 91:3465-3473.

Ando T, Uchihashi T, Kodera N, Yamamoto D, Miyagi A, Taniguchi M, Yamashita H (2008) High-speed AFM and nano-visualization of biomolecular processes. Pflugers Arch 456:211-225.

Ashkin A (1970) Acceleration and trapping of particles by radiation pressure. Phys Rev Lett 24:156-159.

Ashkin A, Dziedzic JM, Bjorkholm JE, Chu S (1986) Observation of a single-beam gradient force optical trap for dielectric particles. Optics Lett 11:288-290.

Ashkin A, Dziedzic JM (1989) Optical trapping and manipulation of single living cells using infra-red laser beams. Ber Bunsenges Phys Chem 93:254-260

Bálint Z, Krizbai IA, Wilhelm I, Farkas EA, Párducz Á, Szegletes Z, Váró G (2007a) Changes induced by hyperosmotic mannitol in cerebral endothelial cells: an atomic force microscopic study. Eur Biophys J 36:113-120.

Bálint Z, Végh AG, Popescu A, Dima M, Ganea C, Váró G (2007b) Direct observation of protein motion during the photochemical reaction cycle of bacteriorhodopsin. Langmuir 23:7225-7228.

Batchelor GK (2000) An Introduction to Fluid Dynamics. Cambridge Mathematical Library Series, Cambridge University Press, Cambridge.

Benoit M, Selhuber-Unkel C (2011) Measuring cell adhesion forces: theory and principles. In Braga PC, Ricci D, eds., Atomic Force Microscopy in Biomedical Research. Humana Press, New York, pp. 355-377.

Bertseva E, Grebenkov D, Schmidhauser P, Gribkova S, Jeney S, Forró L (2012) Optical trapping microrheology in cultured human cells. Eur Phys J E 35:63.

Binnig G, Quate CF, Gerber C (1986) Atomic force microscope. Phys Rev Lett 56:930-933.

Bizzarri AR, Cannistraro S (2010) The application of atomic force spectroscopy to the study of biological complexes undergoing a biorecognition process. Chem Soc Rev 39:734-749.

Boedicker JQ, Vincent ME, Ismagilov RF (2009) Microfluidic confinement of single cells of bacteria in small volumes initiates high-density behavior of quorum sensing and growth and reveals its variability. Angew Chem Int Edit 48:5908-5911.

Carl P, Schillers H (2008) Elasticity measurement of living cells with an atomic force microscope: data acquisition and processing. Pflugers Arch 457:551-559.

Carnegie DJ, Stevenson DJ, Mazilu M, Gunn-Moore F, Dholakia K (2008) Guided neuronal growth using optical line traps. Opt Express 16:10507-10517.

Cetin M, Ucar E, Guven O, Ocak S (2009) Community-acquired urinary tract infections in southern Turkey: etiology and antimicrobial resistance. Clin Nephrol 71:30-35.

Chamberlain AK, MacPhee CE, Zurdo J, Morozova-Roche LA, Hill HA, Dobson CM, Davis JJ (2000) Ultrastructural organization of amyloid fibrils by atomic force microscopy. Biophys J 79:3282-3293.

Chiti F, Dobson CM (2006) Protein misfolding, functional amyloid, and human disease. Annu Rev Biochem 75:333-366.

Cisneros DA, Hung C, Franz CM, Muller DJ (2006) Observing growth steps of collagen self-assembly by time-lapse high-resolution atomic force microscopy. J Struct Biol 154:232-245.

Coles JM, Blum JJ, Jay GD, Darling EM, Guilak F, Zauscher S (2008) In situ friction measurement on murine cartilage by atomic force microscopy. J Biomech 41:541-548.

Constable A, Kim J, Mervis J, Zarinetchi F, Prentiss M (1993) Demonstration of a fiber-optical light-force trap. Opt Lett 18:1867-1869

Cross SE, Jin YS, Rao J, Gimzewski JK (2007) Nanomechanical analysis of cells from cancer patients. Nat Nanotechnol 2:780-783.

Davis ZJ, Abadal G, Hansen O, Borise X, Barniol N, Perez-Murano F, Boisen A (2003) AFM lithography of aluminum for fabrication of nanomechanical systems. Ultramicroscopy 97:467-472.

Deckert-Gaudig T, Deckert V (2011) Nanoscale structural analysis using tip-enhanced Raman spectroscopy. Curr Opin Chem Biol 15:719-724.

de Oteyza DG, Gorman P, Chen YC, Wickenburg S, Riss A,

Mowbray DJ, Etkin G, Pedramrazi Z, Tsai HZ, Rubio A, Crommie MF, Fischer FR (2013) Direct imaging of covalent bond structure in single-molecule chemical reactions. Science 340:1434-1437.

Diao J, Young L, Kim S, Fogarty EA, Heilman SM, Zhou P, Shuler ML, Wu M, DeLisa MP (2006) A three-channel microfluidic device for generating static linear gradients and its application to the quantitative analysis of bacterial chemotaxis. Lab Chip 6:381-388.

Di Leonardo R, Búzás A, Kelemen L, Vizsnyiczai G, Oroszi L, Ormos P (2012) Hydrodynamic synchronization of light driven microrotors. Phys Rev Lett 109:034104.

Dulinska I, Targosz M, Strojny W, Lekka M, Czuba P, Balwierz W, Szymonski M (2006) Stiffness of normal and pathological erythrocytes studied by means of atomic force microscopy. J Biochem Biophys Methods 66:1-11.

Englert DL, Manson MD, Jayaraman A (2010) Investigation of bacterial chemotaxis in flow-based microfluidic devices. Nat Protoc 5:864–872.

Florin EL, Moy VT, Gaub HE (1994) Adhesion forces between individual ligand-receptor pairs. Science 264:415-417.

Foxman B, Ki M, Brown P (2007) Antibiotic resistance and pyelonephritis. Clin Infect Dis 45:281-283.

Franz CM, Puech PH (2008) Atomic force microscopy: a versatile tool for studying cell morphology, adhesion and mechanics. Cell Mol Bioeng 1:289-300.

Guck J, Ananthakrishnan R, Mahmood H, Moon TJ, Cunningham CC, Kas J (2001) The optical stretcher: a novel laser tool to micromanipulate cells. Biophys J 81:767-784.

Gad M, Itoh A, Ikai A (1997) Mapping cell wall polysaccharides of living microbial cells using atomic force microscopy. Cell Biol Int 21:697-706.

Hol FJH, Galajda P, Nagy K, Woolthuis RG, Dekker C, Keymer JE (2013) Spatial structure facilitates cooperation in a social dilemma: empirical evidence from a bacterial community. PLoS ONE 8:e77042.

Holman JP (2002) Heat transfer. McGraw-Hill, New York, p. 207.

Huh D, Matthews BD, Mammoto A, Montoya-Zavala M, Hsin HY, Ingber DE (2010) Reconstituting organ-level lung functions on a chip. Science 328:1662-1668.

Huh D, Torisawa YS, Hamilton GA, Kim HJ, Ingber DE (2012) Microengineered physiological biomimicry: organs-on-chips. Lab Chip 12:2156-2164.

Iyer S, Gaikwad RM, Subba-Rao V, Woodworth CD, Sokolov I (2009) Atomic force microscopy detects differences in the surface brush of normal and cancerous cells. Nat Nanotechnol 4:389-393.

Kawata S, Sun H-B, Tanaka T, Takada K (2001) Finer features for functional microdevices. Nature 412:697-698.

Kedrov A, Janovjak H, Sapra KT, Muller DJ (2007) Deciphering molecular interactions of native membrane proteins by single-molecule force spectroscopy. Annu Rev Biophys Biomol Struct 36:233-260.

Kellermayer MS (2011) Combined atomic force microscopy and fluorescence microscopy. In Braga PC, Ricci D, eds., Atomic Force Microscopy in Biomedical Research. Humana Press, New York, pp. 439-456.

Keymer JE, Galajda P, Muldoon C, Park S, Austin RH (2006) Bacterial metapopulations in nanofabricated landscapes. Proc Natl Acad Sci USA 103:17290-17295.

Kim L, Vahey MD, Lee HY, Voldman J (2006) Microfluidic arrays for logarithmically perfused embryonic stem cell culture. Lab Chip 6:394-406.

Kirby BJ (2010) Micro- and Nanoscale Fluid Mechanics: Transport in Microfluidic Devices. Cambridge University Press, Cambridge.

Kumar S, LeDuc PR (2009) Dissecting the molecular basis of the mechanics of living cells. Exp Mech 49:11-23.

Kumar S, Weaver VM (2009) Mechanics, malignancy, and metastasis: The force journey of a tumor cell. Cancer Metast Rev 20:113-127.

Lacapere JJ, Pebay-Peyroula E, Neumann JM, Etchebest C (2007) Determining membrane protein structures: still a challenge! Trends Biochem Sci 32:259-270.

Li QS, Lee GY, Ong CN, Lim CT (2008) AFM indentation study of breast cancer cells. Biochem Biophys Res Commun 374:609-613.

Li T, Kheifets S, Raizen MG (2011) Millikelvin cooling of an optically trapped microsphere in vacuum. Nat Phys 7:527-530.

Li X, Ballerini DR, Shen W (2012) A perspective on paper-based microfluidics: current status and future trends. Biomicrofluidics 6:011301.

Liang H, Vu KT, Krishnan P, Trang TC, Shin D, Kimel S, Berns MW (1996) Wavelength dependence of cell cloning efficiency after optical trapping. Biophys J 70:1529-1533.

Liphardt J, Onoa B, Smith SB, Tinoco I Jr, Bustamante C (2001) Reversible unfolding of single RNA molecules by mechanical force. Science 292:733-737.

Liu Y, Pinzon-Arango PA, Gallardo-Moreno AM, Camesano TA (2010) Direct adhesion force measurements between *E. coli* and human uroepithelial cells in cranberry juice cocktail. Mol Nutr Food Res 54:1744-1752.

Lu H, Koo LY, Wang WM, Lauffenburger DA, Griffith LG, Jensen KF (2004) Microfluidic shear devices for quantitative analysis of cell adhesion. Anal Chem 76:5257-5264.

Mao H, Cremer PS, Manson MD (2003) A sensitive, versatile microfluidic assay for bacterial chemotaxis. Proc Natl Acad Sci USA 100:5449-5454.

Marcy Y, Ouverney C, Bik EM, Losekann T, Ivanova N, Martin HG, Szeto E, Platt D, Hugenholtz P, Relman DA, Quake SR (2007) Dissecting biological dark matter: single

cell genetic analysis of TM7, a rare and uncultivated microbe from the human mouth. Proc Natl Acad Sci USA 104:11889-11894.

Martin M, Benzina O, Szabo V, Vegh AG, Lucas O, Cloitre T, Scamps F, Gergely C (2013) Morphology and nanomechanics of sensory neurons growth cones following peripheral nerve injury. PLoS One 8:e56286.

Martinez AW, Phillips ST, Butte MJ, Whitesides GM (2007) Patterned paper as a platform for inexpensive, low-volume, portable bioassays. Angew Chem Int Edit 46:1318–1320.

Männik J, Driessen R, Galajda P, Keymer JE, Dekker C (2009) Bacterial growth and motility in sub-micron constrictions. Proc Natl Acad Sci USA 106:14861-14866.

Männik J, Wu F, Hol FJH, Bissichia P, Sherratt D, Keymer JE, Dekker C (2012) Robustness and accuracy of cell division in *Escherichia coli* in diverse cell shapes. Proc Natl Acad Sci USA 109:6957-6962.

Meyer G, Amer MN (1988) Novel optical approach to atomic force microscopy. Appl Phys Lett 53:1045-1047.

Mistry NS, Power R, Anand S, McGloin D, Almohamedi A, Downie M, Reid JP, Hudson AJ, (2012) Analysis of optical trap mediated aerosol coalescence. SPIE Proc 8458, 84582B.

Moreno-Flores S, Benitez R, Vivanco M, Toca-Herrera JL (2010) Stress relaxation and creep on living cells with the atomic force microscope: a means to calculate elastic moduli and viscosities of cell components. Nanotechnology 21:445101.

Moy VT, Florin EL, Gaub HE (1994) Intermolecular forces and energies between ligands and receptors. Science 266:257-259.

Muller DJ (2008) AFM: a nanotool in membrane biology. Biochemistry 47:7986-7998.

Norden AD, Wen PY, Kesari S (2005) Brain metastases. Curr Opin Neurol 18:654-661.

Oroszi L, Galajda P, Kirei H, Bottka S, Ormos P (2006) Direct measurement of torque in an optical trap and its application to double-strand DNA. Phys Rev Lett 97:058301.

Palima D, Bañas AR, Vizsnyiczai G, Kelemen L, Ormos P, Glückstad J (2012) Wave-guided optical waveguides. Opt Express 20:2004-2014.

Perkins TT, Quake SR, Smith DE, Chu S (1994) Relaxation of a single DNA molecule observed by optical microscopy. Science 264:822-825.

Phillips DB, Gibson GM, Bowman R, Padgett MJ, Hanna S, Carberry DM, Miles MJ, Simpson SH (2012a) An optically actuated surface scanning probe. Opt Express 20:29679-29693.

Phillips DB, Simpson SH, Grieve JA, Bowman R, Gibson GM, Padgett MJ, Rarity JG, Hanna S, Miles MJ, Carberry DM (2012b) Force sensing with a shaped dielectric microtool. Europhys Lett 99:58004.

Picco LM, Bozec L, Ulcinas A, Engledew DJ, Antognozzi M, Horton MA, Miles MJ (2007) Breaking the speed limit with atomic force microscopy. Nanotech 18:044030.

Power RM, Reid JP (2014) Probing the micro-rheological properties of aerosol particles using optical tweezers. Rep Prog Phys 77:074601.

Qin D, Xia Y, Whitesides GM (2010) Soft lithography for micro- and nanoscale patterning. Nat Protoc 5:491-502.

Rao S, Bálint S, Cossins B, Guallar V, Petrov D (2009) Raman study of mechanically induced oxygenation state transition of red blood cells using optical tweezers. Biophys J 96:209-216.

Rief M, Oesterhelt F, Heymann B, Gaub HE (1997) Single molecule force spectroscopy on polysaccharides by atomic force microscopy. Science 275:1295-1297.

Robert P, Sengupta K, Puech PH, Bongrand P, Limozin L (2008) Tuning the formation and rupture of single ligand-receptor bonds by hyaluronan-induced repulsion. Biophys J 95:3999-4012.

Shaffrey ME, Mut M, Asher AL, Burri SH, Chahlavi A, Chang SM, Farace E, Fiveash JB, Lang FF, Lopes MB, Markert JM, Schiff D, Siomin V, Tatter SB, Vogelbaum MA (2004) Brain metastases. Curr Probl Surg 41:665-741.

Shepherd GM, Corey DP, Block SM (1990) Actin cores of hair-cell stereocilia support myosin motility. Proc Natl Acad Sci USA 87:8627-8631

Smith DE, Tans SJ, Smith SB, Grimes S, Anderson DL, Bustamante C (2001) The bacteriophage phi29 portal motor can package DNA against a large internal force. Nature 413:748-752.

Starzyk D, Korbut R, Gryglewski RJ (1999) Effects of nitric oxide and prostacyclin on deformability and aggregability of red blood cells of rats ex vivo and in vitro. J Physiol Pharmacol 50:629-637.

Stoodley P, deBeer D, Lewandowski Z (1994) Liquid flow in biofilm systems. Appl Envir Microbiol 60:2711-2716.

Sundd P, Pospieszalska MK, Ley K (2013) Neutrophil rolling at high shear: flattening, catch bond behavior, tethers and slings. Mol Immunol 55:59-69.

Suresh S (2007) Biomechanics and biophysics of cancer cells. Acta Biomater 3:413-438.

Tam JM, Castro CE, Heath RJW, Cardenas ML, Xavier RJ, Lang MJ, Vyas KM (2010) Control and manipulation of pathogens with an optical trap for live cell imaging of intercellular interactions. PLoS ONE 5:e15215.

Ubbink J, Schar-Zammaretti P (2005) Probing bacterial interactions: integrated approaches combining atomic force microscopy, electron microscopy and biophysical techniques. Micron 36:293-320.

Unger MA, Chou H, Thorsen T, Scherer A, Quake SR (2000) Monolithic microfabricated valves and pumps by multilayer soft lithography. Science 288:113-116.

Végh AG, Nagy K, Bálint Z, Kerényi A, Rákhely G, Váró

G, Szegletes Z (2011a) Effect of antimicrobial peptide-amide: indolicidin on biological membranes. J Biomed Biotechnol 2011:670589.

Végh AG, Fazakas C, Nagy K, Wilhelm I, Krizbai IA, Nagy szi P, Szegletes Z, Váró G (2011b) Spatial and temporal dependence of the cerebral endothelial cells elasticity. J Mol Recognit 24:422-428.

Végh AG, Fazakas C, Nagy K, Wilhelm I, Molnár J, Krizbai IA, Szegletes Z, Váró G (2012) Adhesion and stress relaxation forces between melanoma and cerebral endothelial cells. Eur Biophys J 41:139-145.

Vinckier A, Semenza G (1998) Measuring elasticity of biological materials by atomic force microscopy. FEBS Lett 430:12-16.

Wojcikiewicz EP, Abdulreda MH, Zhang X, Moy VT (2006) Force spectroscopy of LFA-1 and its ligands, ICAM-1 and ICAM-2. Biomacromol 7:3188-3195.

Yuan C, Chen A, Kolb P, Moy VT (2000) Energy landscape of streptavidin-biotin complexes measured by atomic force microscopy. Biochem 39:10219-10223.

Zhang H, Liu K-K (2008) Optical tweezers for single cells. J R Soc Interface 5:671–690.

Zhang Q, Lambert G, Liao D, Kim H, Robin K, Tung C, Pourmand N, Austin RH (2011) Acceleration of emergence of bacterial antibiotic resistance in connected microenvironments. Science 333:1764-1767.

Zhang T, Chao Y, Shih K, Li XY, Fang HH (2011) Quantification of the lateral detachment force for bacterial cells using atomic force microscope and centrifugation. Ultramicroscopy 111:131-139.